Investigations on the Determinants Responsible for Low Molar Mass Dextran Formation by DSR-M Dextransucrase

Marion Claverie, Gianluca Cioci, Marlène Vuillemin, Nelly Monties, Pierre Roblin, Guy Lippens, Magali Remaud Simeon, Claire Moulis

Investigations on the Determinants Responsible for Low Molar Mass Dextran Formation by DSR-M Dextransucrase

Marion Claverie,[†] Gianluca Cioci,[†] Marlène Vuillemin,[†] Nelly Monties,[†] Pierre Roblin,[‡] Guy Lippens,[†] Magali Remaud-Simeon,*[,†] and Claire Moulis*[,†]

[†]LISBP, Université de Toulouse, CNRS, INRA, INSA, Toulouse, France

[‡]Université de Toulouse, LGC UMR 5503 (CNRS/UPS/INPT), 118 route de Narbonne 31062 Toulouse, France

ABSTRACT: Certain enzymes of the GH70 family dextransucrases synthesize very high molar mass dextran polymers, whereas others produce a mixed population of very high and low molar mass products directly from sucrose substrate. Identifying the determinants dictating polymer elongation would allow the tight control of dextran size. To explore this central question, we focus on the recently discovered DSR-M enzyme from *Leuconostoc citreum* NRRL B-1299, which is the sole enzyme that naturally, exclusively, and very efficiently produces only low molar mass dextrans from sucrose. Extensive biochemical and structural characterization of a truncated form of DSR-M (DSR-MΔ2, displaying the same biochemical behavior as the parental enzyme) and X-ray structural analysis of complexes with sucrose and isomaltotetraose molecules together with accurate monitoring of the resulting polymer formation reveal that DSR-MΔ2 adopts a nonprocessive mechanism attributed to (i) a high propensity to recognize sucrose as a preferred acceptor at the initial stage of catalysis, (ii) an ability to elongate oligodextrans irrespective of their size, and (iii) the presence of a domain V showing a weak ability to bind to the growing dextran chains. In this study, we present the 3D structure with the largest defined domain V reported to date in the GH70 family and map sugar binding pockets on the basis of the structure of the complex obtained with isomaltotetraose. Altogether, these findings give insights into the interplay between the domain V and the catalytic site during polymerization. They open promising strategies for GH70 enzyme engineering aiming at modulating glucan size.

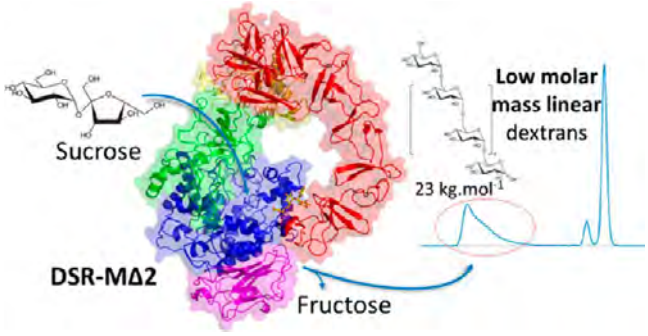

KEYWORDS: *glucansucrases, dextransucrases, dextran, crystal structure, GH70 family, nonprocessive polymerization, glucan-binding domain, carbohydrate-binding protein*

INTRODUCTION

Glucansucrases (GS) from the glycoside hydrolase family 70 (GH70) are α-transglucosylases found in lactic acid bacteria (LAB) such as *Leuconostoc*, *Lactobacillus*, *Streptococcus*, and *Weissella*.[1−3] From sucrose, an economical and abundant agricultural resource, they catalyze the polymerization of the glucosyl units to form homopolymers of variable size and structure, notably with different types of α-osidic bonds and degrees of branching. Among the resulting polymers, dextrans contain more than 50% of α-(1→6) linkages and usually display a very high molar mass (HMM) (10^6−10^8 g mol^{-1}). The linear dextrans (more than 95% of α-(1→6) osidic bonds) were the first microbial polysaccharides to find industrial applications as infusion fluids, volume expanders, iron carriers, anticoagulants, and vaccine adjuvants after derivatization.[4,5] These applications mainly concern dextran fractions of average molar mass of 1 × 10^3, 10 × 10^3, 40 × 10^3, or 70 × 10^3 g mol^{-1}, obtained by partial acid hydrolysis and solvent fractionation of the native polymer produced by fermentation.[6] Dextran70 (70 × 10^3 g mol^{-1}) is referenced in the List of Essential Medicines by the World Health Organization (19th WHO model List of Essential Medicines, 2015). The chemical processes behind the production of these clinical fractions require several steps and are, consequently, quite costly, time-consuming, and non-eco-friendly,[7,5] stimulating the search for alternative and greener processes. Dextransucrase and dextranase activities have for example been combined to develop a one-step synthetic process of low molar mass dextrans.[8−12] Reactions in the presence of sucrose and sugar acceptors such as glucose and maltose were also investigated to favor the synthesis of low molar mass dextrans, but these conditions never totally suppressed the formation of high molar mass polymers.[13−15]

Control of the size and structure of the polymers synthesized by glucansucrases would benefit from a better comprehension of the polymerization mechanism and, in particular, of the protein structural determinants involved in polymer size

DOI: 10.1021/acscatal.7b02182

control or linkage specificity. Glucansucrases as flexible proteins of high molecular weight (~150−200 kDa) are difficult to crystallize, and for years structure/function relationships were essentially based on primary structure analyses. However, quite recently, three 3D structures of truncated GH70 glucansucrases differing in their linkage specificity were solved: GTF180-ΔN from *Lactobacillus reuteri* 180,[16] GTFA-ΔN from *L. reuteri* 121,[17] and GTF-SI from *Streptococcus mutans* MT8148.[18] Two additional crystal structures of GH70 enzymes complete the picture: that of ΔN123-GBD-CD2, a representative of the branching sucrase subgroup specialized in dextran branching,[19,20] and that of Gtf-B-ΔNΔV from *L. reuteri* 121, a representative of the 4,6-α-glucanotransferase subgroup, which uses maltooligosaccharides as donors instead of sucrose.[21] All structures have in common a five-domain organization with a global U-shaped folding. Domains A−C are also found in related GH13 enzymes, which form with GH70 and GH77 enzymes the clan GH-H, whereas domains IV and V are unique to the GH70 family. Except for domain C, these domains are formed by two discontinuous segments from both N- and C-terminal polypeptides. The catalytic domain A adopts a $(\beta/\alpha)_8$ barrel fold and contains the three catalytic amino acids involved in the α-retaining mechanism: the aspartate nucleophile and the glutamate acid−base catalyst involved in the β-D-glucosyl enzyme formation, along with the third aspartate acting as a transition state stabilizer.[3,20,22] Sequence comparison combined with structural analyses also suggested the presence of residues involved in linkage specificity in this domain.

Our understanding at the molecular level of how glucansucrases control the size of their polymers is still limited. Indeed, some GSs such as the *L. mesenteroides* NRRL B-512F DSR-S and its variant DSR-S vardel Δ4N (a glucansucrase deleted of a part of the variable region located at N-term and of four N repeats at C-term) are efficient polymerases, producing almost uniquely very HMM glucans (10^8 g mol^{-1}).[23,24] Others, such as the dextransucrase GTF-180 from *Lb. reuteri* 180 or the alternansucrase ASR from *L. mesenteroides* NRRL B-1355 synthesize two glucan populations, the first of very high molar mass (around 10^7 g mol^{-1}) and the other comprising oligosaccharides or polymers of medium size (10^3−10^4 g mol^{-1}).[25−27] Several studies suggest that domain V, located at the N- and C-terminal extremity of the enzymes, plays a role in the polymer size through its capacity to bind glucans.[23,28,29] Indeed, domain V fragments are able to fold independently and strongly bind α-glucans with dissociation constants in the nanomolar range.[28,30−33] Called accordingly the glucan binding domain (GBD), this domain V contains repeated motifs derived from a common YG motif.[34] The available crystal structures of GH70 enzymes unfortunately mostly concern truncated constructs, in which only a small part of the native domain V is visible.[16,19,22] Only very recently, several complexes of the ΔN123-GBD-CD2 branching sucrase with glucose, isomaltose (I2), and isomaltotriose (I3) provided the first structural evidence of sugar binding pockets with a common topology and directly interacting with carbohydrates in domain V.[35] In *L. mesenteroides* NRRL B-512F DSR-S, successive suppressions of these repeat units induced a progressive loss of activity and decrease in the polymer size.[23] The variant deleted of the entire domain V kept only 0.14% activity relative to the native enzyme, totally lost its ability to produce HMM dextran (10^8 g mol^{-1} for the native form), and only synthesized low molar mass (LMM) dextran of about 10^3 g mol^{-1}. In contrast, truncation of the domain V of GTF180-ΔN yielded a catalytically quasi fully active enzyme (only 25% reduction) but induced a change of the distribution between oligosaccharides and HMM dextran populations, a lower amount of glucosyl units being incorporated in HMM polymers (2% for GTF180-ΔN-ΔV versus 16.3% for GTF180-ΔN) to the profit of oligosaccharide synthesis. However, the size of the HMM dextran produced by GTF180-ΔN-ΔV remains unchanged (2×10^7 g mol^{-1}). In addition, the mutation of Leu940 located in the acceptor substrate binding site of GTF180-ΔN-ΔV partially restored its capacity to synthesize HMM polysaccharides, showing that both the active site and the domain V are important in controlling polymer size.[27] Overall, these findings suggest that the role of domain V may vary from one enzyme to another, but structural data to fully understand the interplay between the various domains during polymerization and their implication in the control of the polymer size are still lacking.

To address these questions, the enzyme DSR-M, recently isolated from *L. citreum* NRRL B-1299, is of particular interest.[36] Indeed, in comparison to all GSs characterized to date, this enzyme is the first one reported to naturally synthesize linear LMM dextrans directly from sucrose. As sequence analysis did not reveal any obvious discriminating features that could explain this specificity, we report here the three-dimensional X-ray structures of the protein alone or in complex with either sucrose or isomaltotetraose (I4: [α-D-Glcp-(1→6)]$_3$-Glcp) which were solved at 3.2, 3.6, and 3.7 Å, respectively. The last structure displays the largest structure of a domain V reported so far, in which four putative binding pockets with a topology close to that described in ΔN123-GBD-CD2 branching sucrase could be identified. The complex with I4 further revealed a sugar molecule in one of these pockets, providing a rational basis to explore the role of the GBD in determining the length of the resulting dextrans. Specific loop structures around the catalytic site were further examined by site-directed mutagenesis, and their functional impact was evaluated by analysis of the resulting polymers. From our data, a distributive mode of polymer formation emerges for DSR-M, with an involvement of the domain V to the length of the resulting dextrans.

MATERIALS AND METHODS

Residue numbering refers to the whole size DSR-M enzyme (GenBank accession number: BN964_01347).

Construction of DSR-MΔ1, DSR-MΔ2, and DSR-MΔV Deletion Mutants. *dsrm Δ1*, *dsrm ΔV-Nter*, and *dsrm ΔV* genes were amplified by PCR from pET-55/DsrM plasmid DNA template[36] using the primers described in Table S1 in the Supporting Information. The addition of a CACC sequence (underlined) to the 5′-forward primers allowed the correct insertion of genes into the pENTR/D-TOPO vector (Life Technologies, Carlsbad, CA, USA). From a positive entry clone, LR recombination (Gateway LR Clonase II enzyme mix, Life Technologies) was performed with pET-55-DEST destination vector (Novagen). Expression clones were selected on LB agar plates supplemented with 100 μg mL^{-1} of ampicillin. Plasmids were extracted with a Sigma-Aldrich GenElute HP Plasmid Miniprep kit, verified by restriction analyses, and the genes of interest were sequenced (GATC Biotech, Constance, Germany). *E. coli* TOP10 competent cells (Life Technologies) were used for all cloning experiments. Concerning the construction of DSR-MΔ2 (form corresponding to the crystallized protein), the deletion of the first 151

amino acids (including the strep tag) from DSR-MΔ1 was performed following the method described by Wang and Malcolm[37] (primers in Table S1). Briefly, this method consists of the use of a two-stage procedure, based on the QuikChange Site-Directed Mutagenesis protocol (Stratagene, La Jolla, CA, USA), in which a pre-PCR, single-primer extension stage before the standard protocol allows the deletion of a sequence of interest.

Protein Expression and Purification. Transformed *E. coli* BL21 star DE3 cells were grown in modified ZYM5052[38] (with the following changes: 0.1% lactose, 0% glucose, and 1% glycerol), supplemented with ampicillin (100 μg mL^{-1}) at 21 °C with agitation (150 rpm). After 26 h of incubation, cells were harvested by centrifugation, resuspended in lysis buffer (20 mM phosphate sodium buffer, pH 7.4, 500 mM NaCl, 20 mM imidazole) supplemented with EDTA free antiprotease tablets (Roche, Basel, Switzerland), and disrupted by sonication. After centrifugation, recombinant enzymes were recovered in the soluble fraction of the crude cell extract, ready for purification.

Protein purification was performed using the ÄKTAxpress (GE Healthcare, Little Chalfont, U.K.) at 8 °C, with a first step consisting of His6 tag affinity chromatography (for details, see ref 39) followed by a size exclusion step on a Superose 12 column 16 × 60 (GE Healthcare) from which the protein preparation is eluted with crystallization buffer (30 mM MES pH 6.5, 100 mM NaCl, 0.05 g L^{-1} $CaCl_2$), or with 50 mM sodium acetate buffer (pH 5.75, 100 mM NaCl, 0.05 g L^{-1} $CaCl_2$) for biochemical characterization. Protein purity was verified by SDS-Page gel electrophoresis. Protein concentration was estimated by spectroscopy at 280 nm, using a NanoDrop instrument (Wilmington, DE, USA). Theoretical molar extinction coefficients and molecular weights were calculated using the ExPASy ProtParam tool (http://web.expasy.org/protparam).

Activity Assays. Activity was assayed using the 3,5-dinitrosalicylic method.[40] One unit of DSR-M variant is defined as the amount of enzyme that catalyzes at 30 °C the production of 1 μmol of fructose per minute, from 292 mM sucrose, in 50 mM sodium acetate buffer pH 5.75.

Enzymatic Reaction and Product Characterization. Enzymatic reactions were performed at 30 °C on 292 mM sucrose in 50 mM sodium acetate buffer at pH 5.75, using 1 U mL^{-1} enzyme (corresponding to 0.014 mg mL^{-1} for DSR-MΔ2), stopped by 5 min incubation at 95 °C, and samples were stored at −20 °C until further analyses. For kinetic studies, samples were taken at regular intervals until total sucrose depletion. The reaction mixtures were then analyzed by HPAEC-PAD and HPSEC.

HPAEC-PAD (high-performance anion exchange chromatography with pulsed amperometric detection) analyses were performed using a CarboPac TM PA100 analytical column (2 mm × 250 mm) coupled with a CarboPacTM PA100 guard (2 mm × 50 mm). Glucose, fructose, leucrose (5-0-α-D-glucopyranosyl-D-fructose), and sucrose were separated using a sodium acetate gradient (6−500 mM) in 150 mM NaOH over 36 min (0.250 mL min^{-1}), and quantification was performed using standards of these sugars at 5, 10, 15, and 20 mg kg^{-1}. Calculation of the percentages of glucosyl moieties derived from sucrose and incorporated into free glucose (%$G_{glucose}$) or leucrose (%$G_{leucrose}$) was done using molar concentrations at the initial and final times of the reaction (t_0 and t_f): %$G_{glucose}$ = [glucose$_{t_f}$]/[sucrose$_{t_0}$] and %$G_{leucrose}$ = [leucrose$_{t_f}$]/[sucrose$_{t_0}$]. Longer sodium acetate gradients varying from 50 to 136 min were used for oligosaccharide content analyses.

HPSEC analyses were performed using Shodex OH-Pak SB-804 and SB-802.5 columns (Showa Denko, Minato-ki, Tokyo, Japan) in series, coupled with a Shodex OH-Pak SB-G guard column and placed in a 30 °C oven. Samples were diluted in water to a maximum of 10 g kg^{-1} of total sugars. Elution with water was performed at a flow rate of 0.3 mL min^{-1}. After total sucrose consumption, the percentage of glucosyl residues from sucrose incorporated into polymer (%$G_{dextran}$ = (342/162) × Area$_{dextran\ t_f}$/Area$_{sucrose\ t_0}$) was calculated. The weight-average molar masses at peak apex of synthesized dextrans were determined using a calibration curve with standards of fructose, sucrose, and dextrans of 1.5, 11.3, 39.1, and 68.4 kg mol^{-1} (Sigma-Aldrich), at 10 g kg^{-1} each.

Crystallization and Data Collection. Freshly purified enzyme was concentrated using a centrifugal filter device (Amicon Ultra, 4 Ultracel, 50 kDa; Millipore). All crystallization experiments were carried out at 12 °C by the sitting-drop vapor-diffusion method, using MRC 96-well microplates (Molecular Dimensions, Newmarket, U.K.) and a Nanodrop ExtY crystallization instrument (Innovadyne Technologies, Santa Rosa, CA, USA) to prepare 400 nL droplets. Initial screening was performed using JSCG+, PACT, and PEGS I&II screens (Qiagen Hilden, Germany), from which we identified one condition in the presence of potassium thiocyanate. After condition optimization, the best DSR-MΔ2 crystals were obtained within a week with a 1/1 (v/v) ratio of protein to precipitant solution (PEG 3350 20%, 0.1 M 1,3-bis[tris-(hydroxymethyl)methylamino]propane pH 6.5, 0.15 M KSCN; protein concentration 20−22 mg mL^{-1}; cryoprotection solution mother liquor + 10% (w/v) glycerol for the apo crystals; PEG 3350 18%, 0.1 M 1,3-bis[tris(hydroxymethyl)-methylamino]propane pH 6.5, 0.225 M KSCN 0.01 M Praseodyne Acetate (additive), protein preparation 4 mg mL^{-1} + 10 mM I6; cryoprotection solution mother liquor + 20% (w/v) ethylene glycol + 50 mM I6 (10 min) for the inactive IMOS-complex; PEG 3350 20%, 0.2 M sodium citrate tribasic dihydrate 0.1 M Bis-Tris propane 6.5 protein preparation 6,00 mg mL^{-1} + 10 mM sucrose + 5 mM $SrCl_2$; cryoprotection solution Cryo 15% ethylene glycol + 10 mM Sacc for the inactive sucrose complex).

Diffraction data were collected at beamlines ID23-2 and ID30-b at the European Synchrotron Radiation Facility (Grenoble, France). The diffraction data were collected at 100 K. The data sets were integrated using XDS[41] and scaled using SCALA from the CCP4 suite.[42] The same set of R_{free} reflections has been generated on the first 3.2 Å data set and transferred to the other data sets.

Structure Determination. The DSR-MΔ2 structure was initially solved at 3.2 Å resolution by molecular replacement with PHASER[43] using the structure of GTF-SI (Protein Data Bank entry 3AIE) as the search model. Manual rebuilding cycles using COOT[44] alternating with restrained refinement using REFMAC5[45] resulted in an incomplete model, lacking an important part (108 residues) of the N-terminal GBD. Residual electron density at the bottom of the catalytic pocket could be attributed to a glycerol molecule coming from the cryobuffer. This model has been deposited as 5LFC at the PDB and was used to solve the structure of the sucrose complex (inactive mutant at 3.6 Å) and of the later obtained I4 complex at 3.7 Å

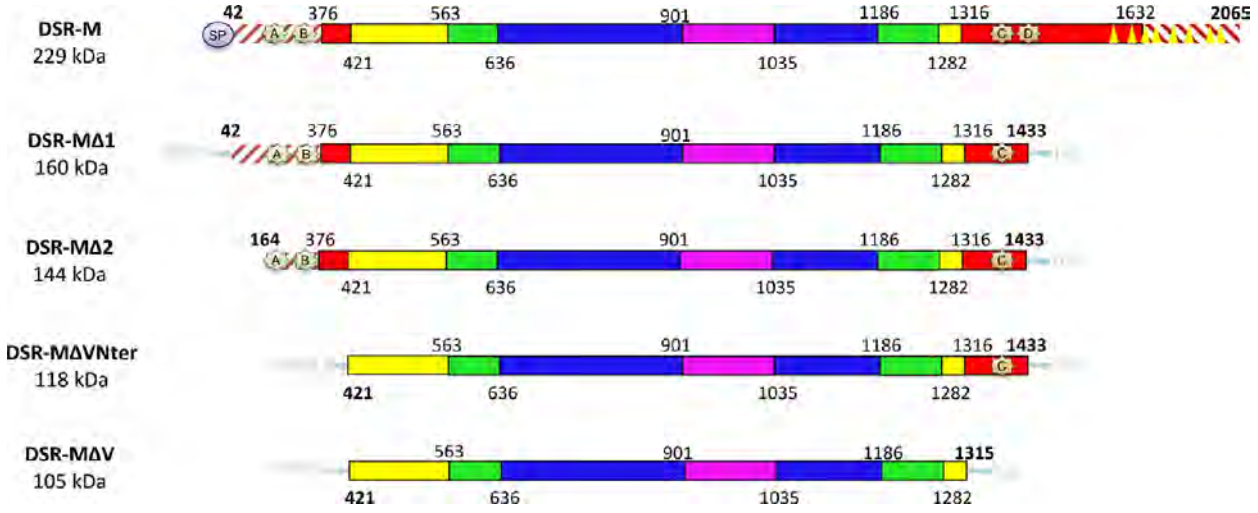

Figure 1. Schematic structural organization of DSR-M and the truncated variants, based on amino acid alignment with GTF-180-ΔN and structural analysis. Hatched red lines correspond to nonaligned zones. DSR-M structural domains: (i) domain V in red; (ii) domain IV in yellow; (iii) domain A in blue; (iv) domain B in green; (v) domain C in magenta. The blue circle represents the signal peptide, APY motifs are indicated with triangles, and pale yellow stars marked as A–D represent putative glucan binding pockets.

resolution. For this last data set, as the N-terminal GBD was entirely visible in the chain A (see Figure S1 in the Supporting Information), its structure has been reconstructed by placing small GBD fragments (obtained by homology modeling) followed by manual rebuilding cycles and refinement. Although the enzyme was cocrystallized and soaked with I6, only four residues were clearly visible in the electron density. The resulting structure will thus be referred to as the I4 complex. The tetrasaccharide was reconstructed by first superimposing the structure of ΔN123-GBD-CD2 in complex with isomaltotriose (4TTU). Praseodymium ions have been modeled as single atoms, as the electron density does not allow the modeling of the metal coordination sphere. Data collection and refinement statistics are presented in Table S2 in the Supporting Information.

The final models have been validated using WHATIF and MOLPROBITY Web servers (http://swift.cmbi.ru.nl/whatif; http://molprobity.biochem.duke.edu/). Coordinates and structure factors have been deposited at the PDB (entries 5LFC, 5NGY, and 5O8L for DSR-MΔ2, DSR-MΔ2-E715Q I4 complex, and DSR-MΔ2-E715Q sucrose complex structures, respectively).

SAXS Measurements and Processing. Small-angle X-ray scattering (SAXS) experiments were performed on the SWING beamline[46] at the SOLEIL synchrotron, Gif-sur-Yvette, France. The wavelength was set to 1.033 Å. A 17 × 17 cm^2 Aviex CCD detector was positioned 1800 mm from the sample, with the direct beam off-center. The resulting exploitable q range was 0.006–0.55 $Å^{-1}$, where $q = 4\pi \sin \theta/\lambda$, considering 2θ as the scattering angle. The samples were circulated in a thermostated quartz capillary with a diameter of 1.5 mm and 10 μm wall thickness positioned inside a vacuum chamber. A 50 μL volume of sample was injected onto a size-exclusion column (Bio SEC3 300, Agilent, Santa Clara, CA, USA) equilibrated in MES buffer (30 mM MES pH 6.5, 100 mM NaCl, 0.05 g L^{-1} $CaCl_2$) using an Agilent high-performance liquid-chromatography (HPLC) system and eluted directly into the SAXS capillary cell at a flow rate of 200 μL min^{-1} and a temperature of 10 °C. SAXS data were collected online throughout the elution time, and a total of 149 frames, each lasting 2 s, was recorded separated by a dead time of 0.5 s between frames. The transmitted intensity was continuously measured with an accuracy of 0.1% using a diode embedded in the beam stop. For each sample, the stability of the associated radius of gyration and the global curve shape in the frames corresponding to the main elution peak were checked, and the resulting selection of curves was averaged as described previously.[47] The recorded curves were normalized to the transmitted intensity and subsequently averaged using FOXTROT. The same protocol was applied to buffer scattering. R_g values were determined by a Guinier fit of the one-dimensional curves using the ATSAS package.[48] The $p(r)$ function was calculated using the GNOM program, and the corresponding ab initio envelopes were calculated using the GASBOR program. The solution model including the N-term and C-term residues was calculated and fitted to the experimental data using the AllosMod-FOXS program (https://modbase.compbio.ucsf.edu/allosmod-foxs/).

Mutagenesis Studies. Mutants E715Q (inactive mutant), Y180A, Y264A, L575W, D813A, and L816A were constructed by inverse PCR (oligo-mediated introduction of site-specific mutations) using *dsrm*-Δ2 plasmid as template and the primers described in Table S1 in the Supporting Information. PCR amplification was carried out with Phusion DNA polymerase (0.5 U) for 16 cycles (95 °C, 15 s; 55 or 60 °C, 20 s; 72 °C, 8 min). The parental plasmid template was digested with DpnI, and PCR products were purified using a Qiaquick spin column, following the manufacturer recommendations. *E. coli* TOP10 cells were transformed with the plasmid. Resulting clones were selected on LB agar plates supplemented with 100 μg mL^{-1} of ampicillin. Plasmids were extracted with a Sigma-Aldrich GenElute HP Plasmid Miniprep kit, verified by restriction analyses, and the genes of interest were sequenced (GATC Biotech). DpnI restriction enzyme and Phusion High-Fidelity DNA Polymerase were purchased from New England Biolabs (Beverly, MA, USA). Oligonucleotides were synthesized by Eurogenetec (Liège, Belgium). *E. coli* BL21 star DE3 cells (Life Technologies) were used as hosts for mutant productions. The reaction products from 292 mM sucrose were analyzed by HPSEC and HPAEC-PAD and compared with those obtained with the wild-type DSR-MΔ2 enzyme.

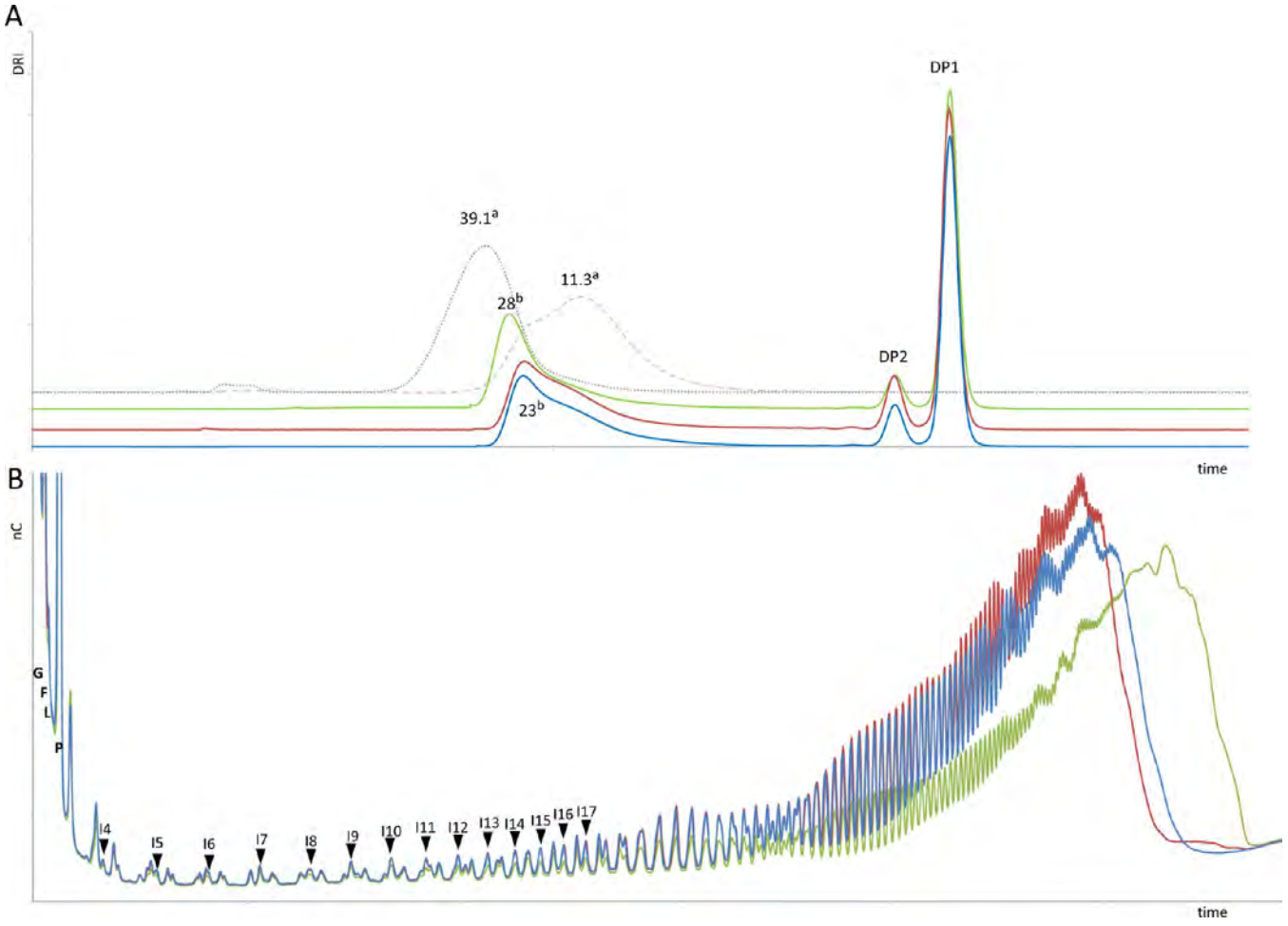

Figure 2. (A) Analysis of the products synthesized by DSR-M variants from 292 mM sucrose. HPSEC chromatogram after total sucrose consumption (green, DSR-M; red, DSR-MΔ1; blue, DSR-MΔ2; gray dash, commercial dextran 11300; gray points, commercial dextran 39100). DP1 denotes monosaccharides and DP2 disaccharides. (B) HPAEC-PAD profile of DSR-MΔ2: G, glucose; F, fructose; L, leucrose; P, palatinose; I4–I20, isomaltooligosaccharides of DP4–DP20. Legend: (a) molar mass of commercial standards in kg mol^{-1}; (b) determined molar mass at peak apex in kg mol^{-1}.

RESULTS

Design and Characterization of Truncated Variants DSR-MΔ1 and DSR-MΔ2. As previously reported, the 229 kDa DSR-M enzyme is among the largest of the GH70 family.[36] On the basis of sequence alignment, the enzyme is predicted to adopt a U-shaped fold resulting in an organization in five domains (Figure 1). In domain V, YG repeats are found at both N- and C-terminal extremities. One particularity is the C-terminal extremity of the protein, where YG repeats are followed by another series of APY repeats nearly identical with those found in the C-terminal region of *L. citreum* NRRL B-1355 alternansucrase (ASR) and *L. citreum* CW28 inulosucrase.[36]

Initial attempts to overexpress the *dsr-M* encoding gene in *E. coli* all led to the production of proteins degraded at their N- and C-terminal extremities. To circumvent this problem, shorter genes were designed and cloned into *E. coli*. DSR-MΔ1 encodes the DSR-M enzyme devoid of its signal peptide and of the last 632 amino acids at its C-terminal extremity (Figure 1). A similar C-terminal truncation of the ASR alternansucrase did not change its enzymatic activity and/or specificity.[26] Production levels of DSR-MΔ1 in *E. coli* BL21 star DE3 reached 10000 U L^{-1} of culture, with a specific activity of 60 U mg^{-1} of protein. The enzyme was purified to homogeneity for crystallization, but SDS-PAGE analysis of the first crystals revealed protein degradation at its N-terminus, also confirmed by Edman sequencing. Thus, an additional removal of 148 amino acids from the DSR-MΔ1 was attempted to construct the DSR-MΔ2 form (Figure 1). For DSR-MΔ2, we obtained 10000 U L^{-1} of culture and determined a specific activity of 67 U mg^{-1} of protein.

With 292 mM sucrose as a starting substrate, HPSEC and HPAEC-PAD reveal that DSR-MΔ1 and DSR-MΔ2 both produce low molar mass dextrans without any trace of very high molar mass polymer (>10^6 g mol^{-1}). On comparison of the polymer distribution of full-length DSR-M and its truncated versions, polymers slightly shorter than those produced by the full enzyme are produced in higher amounts with DSR-MΔ1 and DSR-MΔ2, indicating that the introduced truncations only slightly affect the global product profile (Figure 2 and Table S3 in the Supporting Information). The sucrose hydrolysis ratio is very low (inferior to 4%) for all three enzymes. Moreover, ^{1}H NMR spectra further confirm that these LMM dextrans all contain more than 99% of α-(1→6) linkages; therefore, the truncation does not change the linkage specificity.[36] On this basis, DSR-MΔ2 was considered as a good model to pursue the biochemical and structural characterization.

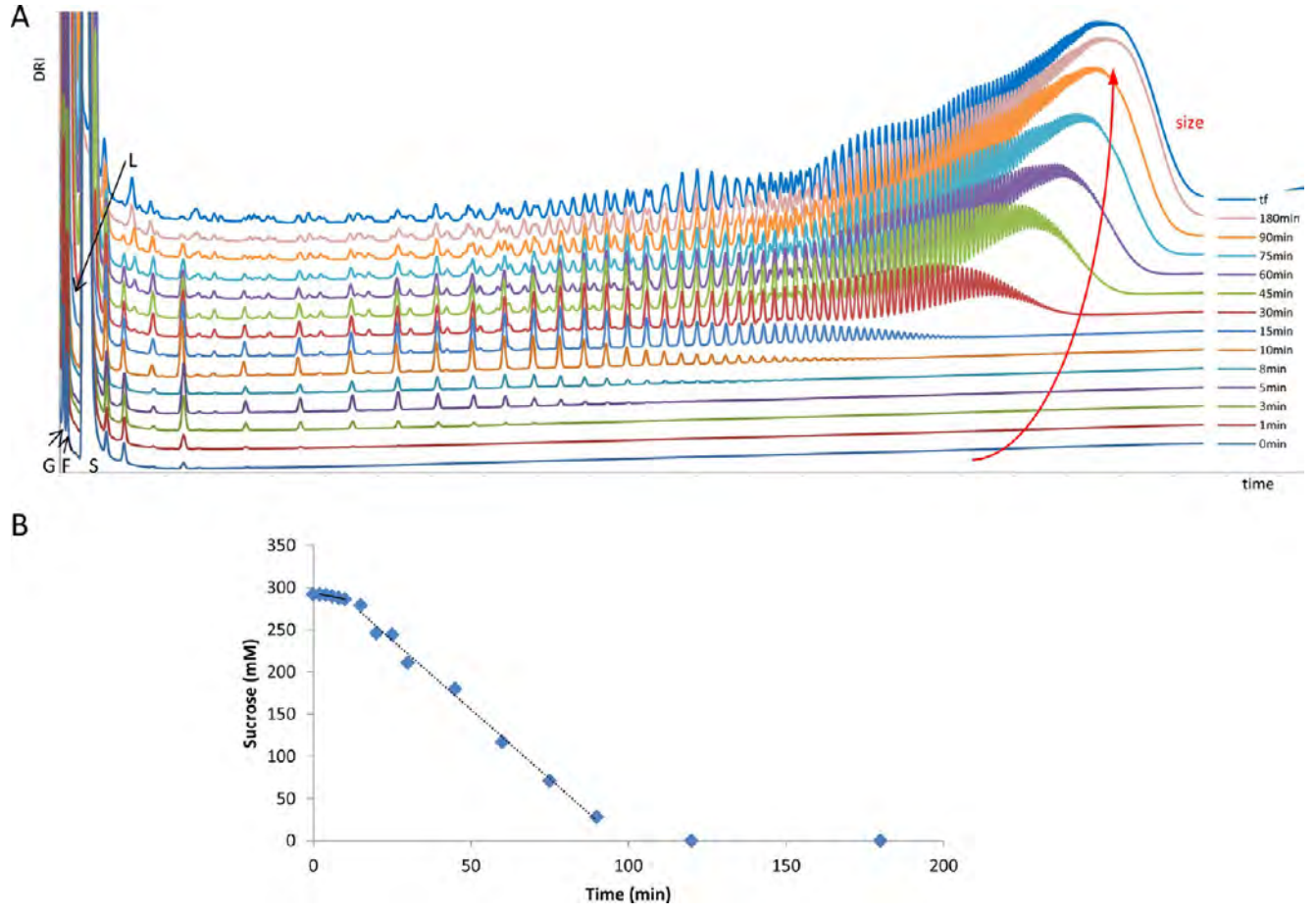

Figure 3. Monitoring of oligosaccharide and polysaccharide production during polymerization catalyzed by DSR-MΔ2: (A) HPAEC-PAD chromatograms during the polymerization reaction (G, glucose; F, fructose; S, sucrose; L, leucrose); (B) sucrose consumption during the reaction.

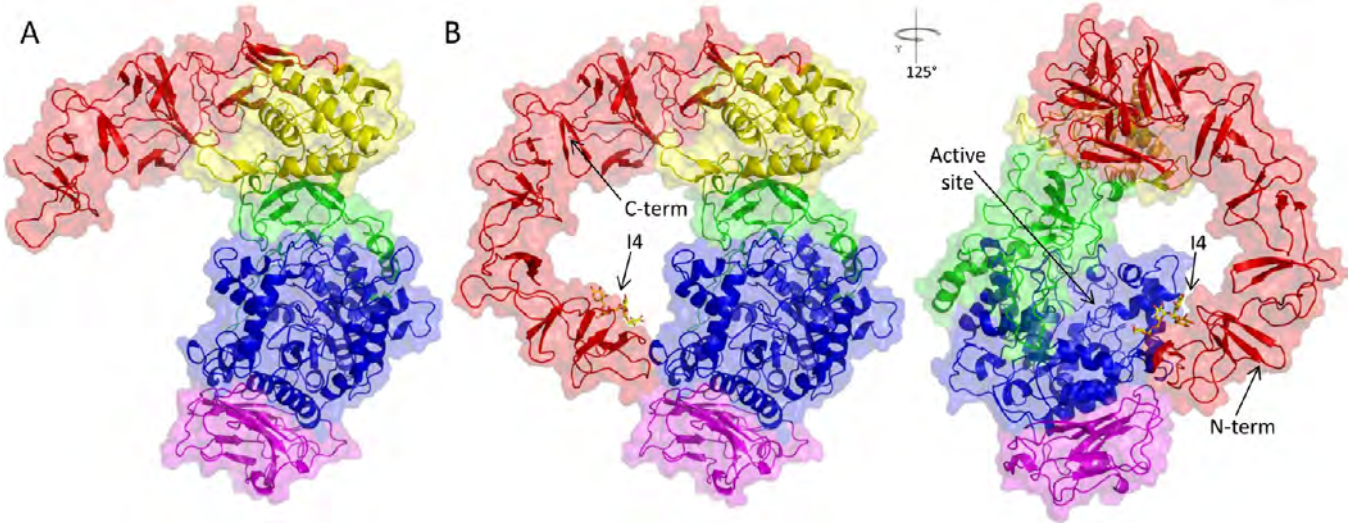

Figure 4. DSRM-Δ2 structures: (A) structure of DSRM-Δ2 solved at 3.2 Å resolution; (B) structure of DSRM-Δ2 E715Q in complex with I4 (inactive mutant) solved at 3.7 Å resolution (magenta, domain C; blue, domain A, which includes the $(\beta/\alpha)_8$ barrel; green, domain B; yellow, domain IV; red, domain V).

Kinetics of Polymer Formation Reveal That DSR-MΔ2 Can Accept Different Chain Initiators. HPAEC monitoring of sucrose consumption and polymer synthesis catalyzed by DSR-MΔ2 from 292 mM sucrose (Figure 3) shows a constant sucrose consumption rate of ~0.76 mM min^{-1} during the first 10 min of reaction, corresponding to 2% of sucrose consumption. In a second phase, from 15 to 90 min, it substantially increases to 3.3 mM min^{-1} before gradually diminishing until the end of the reaction, which is reached within less than 2 h (Figure 3). Oligosaccharides synthesized

during the first reaction step (until 10−15 min) are not isomaltooligosaccharides (IMOS), as judged from their retention times. After incubation with an invertase, they were digested into IMOS (Figure S2 in the Supporting Information). Hence, sucrose is present at the extremity of each oligosaccharide, acting as the chain initiator being glucosylated through the formation of an α-(1→6) linkage onto its glucosyl unit. After the initial reaction phase, the concentration of oligosaccharides of higher DP significantly increases, and IMOS can be detected, showing that glucose (obtained after release onto water) can also be used as a chain initiator. All these produced polymers were efficiently digested by dextranase (Figure S3 in the Supporting Information), confirming the very high content of α-(1→6) linkages determined by NMR. Near the final phase, after 75 min of reaction, two-thirds of sucrose is consumed, leading to a significantly increased fructose concentration. Two additional series of oligosaccharides result from the initial glycosylation of this fructose (leading to sucrose isomers such as leucrose, for example) and their subsequent elongation (Figure S4 in the Supporting Information). At the end of the reaction, 84% of the glucosyl units issued from sucrose are recovered in polymers, 3% in glucose (hydrolysis activity), 8% in leucrose, and 5% in other oligosaccharides of unknown structure and of DP inferior to 12.

3D Structures of DSR-MΔ2 and DSR-MΔ2 E715Q in Complexes with Sucrose or Isomaltotetraose. The structure of the free DSR-MΔ2 (PDB entry: 5LFC) was solved by molecular replacement using GTF-SI as template (PDB entry: 3AIE[18]). In this structure, the 108 residues at the N-term extremity of the domain V were not clearly visible. Two other structures were then obtained: DSR-MΔ2 E715Q in complex with either sucrose in the active site (PDB entry: 5O8L) or isomaltotetraose (I4) (PDB entry: 5NGY). In this latter structure and despite a low resolution, we could manually build the entire N-term part of the domain V in which an I4 molecule could be identified (Figure 4 and Figure S1 in the Supporting Information). For the other GH70 enzymes of known structures, the polypeptide chain adopts a "U-shaped" folding and is organized into five domains: domain A comprising a $(\beta/\alpha)_8$ barrel, domain B (from β-strand 3 to α-helix 3), and domains C, IV, and V.[16,18,19,17,21] Among them, only domain C is formed by a continuous fragment (Figure 4). The final models of DSR-MΔ2 and DSR-MΔ2 E715Q in complex with sucrose comprise residues 288−1436 and 334−1433, respectively. In the structure of DSR-MΔ2 E715Q I4 complex, residues 171−1435 are visible, making it the GH70 structure with the most complete domain V solved to date.

The active site of DSR-MΔ2 in domain A displays a pocket shape at the bottom of a large cavity located at the interface of domains A and B, near which a calcium binding site can be identified at the same position as in the other GH70 glucansucrases.[16,19] Superposition of the structures of the DSR-MΔ2 sucrose complex with that of the GTF180-ΔN sucrose complex (PDB: 3HZ3[16]) shows that conserved residues of the subsites −1 (Arg675, Asp677, Glu715, His789, Asp790, Asn1068, Asp1118, Tyr1127, Asp1178 ,and Gln1183) and +1 (Gln794, Trp717, and Asn681) align well with a 0.23 Å root-mean-square deviation of the Cα. Asp677, Glu715, and Asp790 hence act as the putative nucleophile, general acid/base catalyst, and transition state stabilizer, respectively (Figure 5).

A distinct feature of DSR-MΔ2 is the presence of four loops surrounding its catalytic cleft: namely, loop A1 (located at the N-term part between strand β7 and helix α7), loop A2 connecting strand β2 and helix α2 (Figure 6), and loops B1/B2 (found in the N-terminal part of domain B between strand β3 and helix α3).

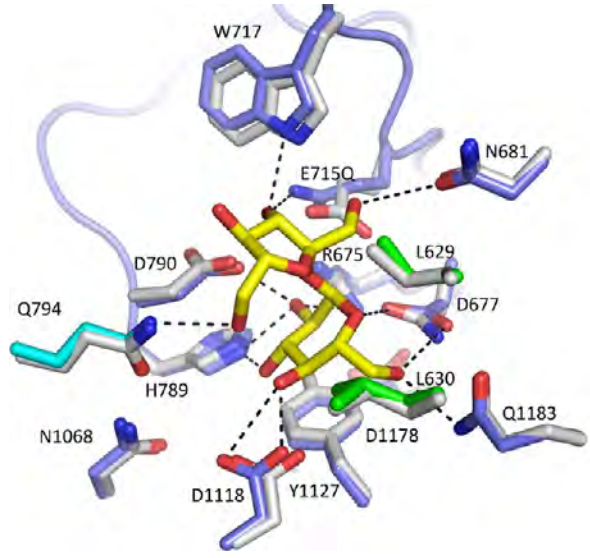

Figure 5. Superposition of subsites −1 and +1 of DSR-MΔ2 E715Q: sucrose complex with subsites −1 and +1 of GTF180-ΔN sucrose complex. The DSR-M catalytic residues are Asp677 (nucleophile), Glu715Gln (acid/base), and Asp790 (transition state stabilizer). Sucrose is shown with yellow carbons. Residues of the inactive GTF180-ΔN mutant (D1025N) that interact with sucrose are represented in gray. The carbon atoms of their structural equivalents in DSR-MΔ2 are shown in blue (domain A), cyan (subdomain H1−H2), and green (domain B).

Loop A1 of DSR-MΔ2 contains a small H1′ helix (residues Val812−Leu817) inserted between the two helices of the subdomain H1−H2 common to other GH70 enzymes. In DSR-MΔ2, this subdomain comprises residues from Gln793 to Gln836 and is located between strand β7 and helix α7 of the $(\beta/\alpha)_8$ barrel. To assess the functional relevance of this insertion, Asp813 and Leu816—two residues of H1′ pointing toward the active site—were mutated into alanine, and the reaction products of the mutant enzymes were analyzed. Although the specific activity of both mutants was 2-fold lower, the resulting product characteristics were not significantly affected by the mutations (Figure S5 and Table S3 in the Supporting Information). When comparing the structures of DSR-MΔ2 sucrose-complex (or of the glycerol complex) with that of the I4-complex, we notice a shift (around 2 Å) of the H1−H2 subdomain with a concomitant reorientation of the Gln794 side chain. This latter residue interacts with the glycerol molecule or fructosyl ring of sucrose in DSR-MΔ2 sucrose complex, respectively, but it is pointing away from the active site in the I4 complex (Figure 7 and Figure S1 in the Supporting Information). Interestingly, a rearrangement of this H1−H2 subdomain with a conformational change of the Gln2326 side chain (equivalent to Gln794 of DSR-MΔ2) was also observed in the structure of ΔN123-GBD-CD2: isomaltotriose complex (4TTU) in comparison with the apoenzyme.[35]

Loop B1 is slightly shorter in DSR-MΔ2 and GTF-SI than in GTF180-ΔN and ΔN123-GBD-CD2 and is very different from its equivalent in Gtf-B. One particularity of B1 in DSR-MΔ2 is its proximity with loop A1 due to the presence of the extra helix

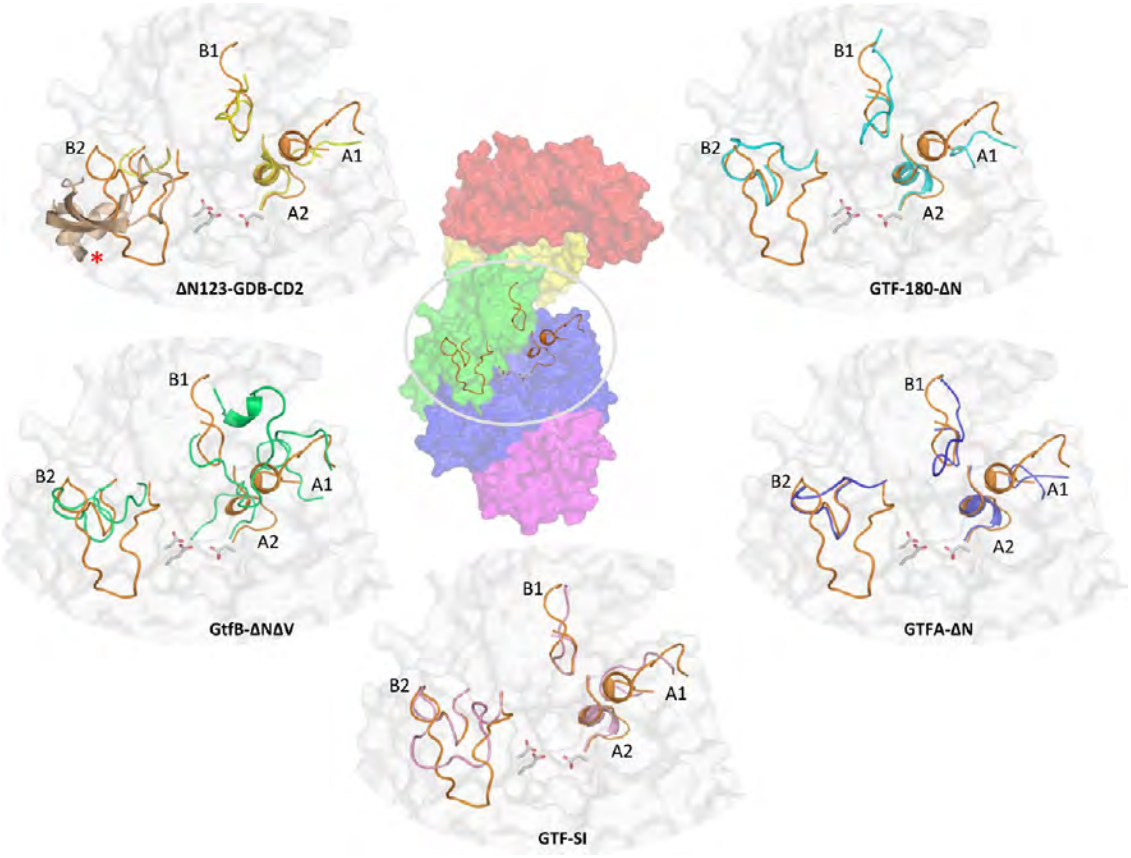

Figure 6. Secondary structure differences between DSR-MΔ2 and other GH70 enzyme structures: (center) DSR-MΔ2 (same colors as in Figure 5) loops A1 (805−820), A2 (1115−1125), B1 (568−578,) and B2 (601−626) in orange; (sides) in yellow, green, pink, blue, and cyan, loops A1, A2, B,1 and B2 of ΔN123-GDB-CD2 (3TTQ), GtfB-ΔNΔV (5JBD), GTF-SI (3AIE), GTFA-ΔN (4AMC), and GTF-180-ΔN (3KLK), respectively, with the surface of DSR-MΔ2 in gray and catalytic residues represented as gray sticks. *Red star: special loop of ΔN123-GDB-CD2 (2731−2796) covering the area of loop B2.*

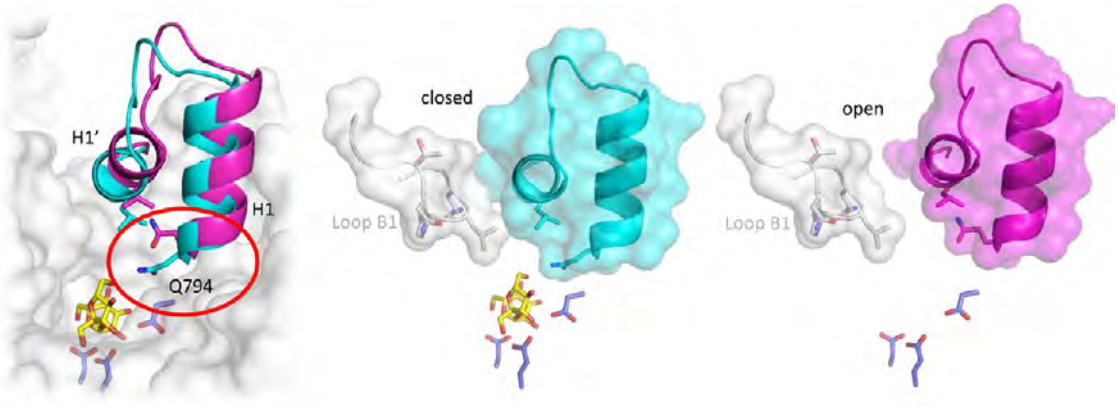

Figure 7. Alternative conformation of Gln794 and subdomain H1−H1′ motion upon sucrose binding in the active site. At the left is shown a superposition of inactive mutant structures in complex with sucrose (cyan) and in complex with I4 (magenta), illustrating the movement of the subdomain H1−H2 and the alternative conformation of Gln794 when sucrose is bound in the active site. "Closed" (middle) and "open" (right) conformations of the catalytic cleft are also represented. The DSR-MΔ2 surface is shown in gray, and catalytic residues and sucrose are represented as blue and yellow sticks, respectively.

H1′. As the loop B1 residue Leu940 of GTF180-ΔN, oriented toward the +1 subsite, was shown[27,49] to be involved in almost every aspect of the polymerization—linkage specificity, hydrolysis activity, size determination, and polysaccharide versus oligosaccharide synthesis ability—the equivalent residue Leu575 in DSR-MΔ2 was replaced by a tryptophan. The mutation resulted in a 50% reduction of dextran molar mass (Table S3 in the Supporting Information) but did not change the linkage specificity. Finally, loop B2 (582−632) of DSR-MΔ2 fills a larger space in comparison to that in the other GH70 enzymes, rendering the binding cleft around the active site less open. Notably, the empty space left by the short (25 amino acids) loop B2 of ΔN123-GBD-CD2 is filled by another

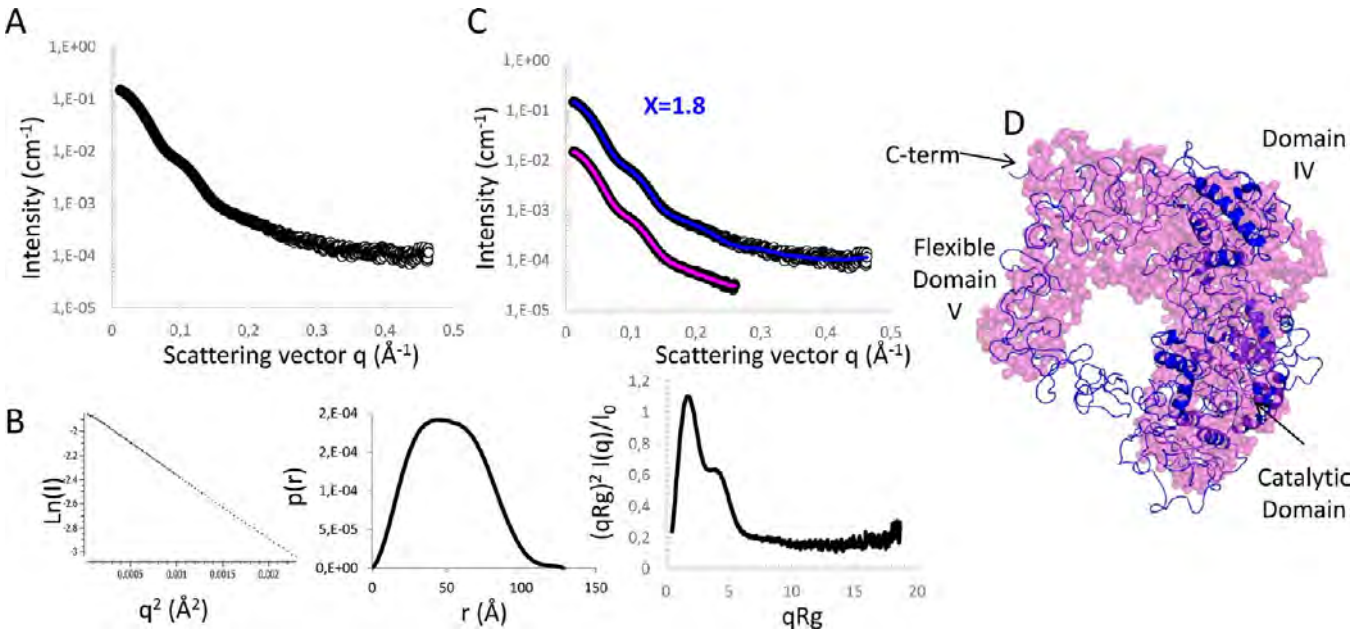

Figure 8. SAXS analysis: (A) scattering curve of DSR-MΔ2; (B) Guinier fit, $P(r)$ function, and dimensionless Kratky plot; (C) fits of the ab initio envelope (purple dots) and of the solution model (blue dots) against the experimental data (black circles).; (D) superposition of the ab initio envelope (purple) and of the solution model (blue).

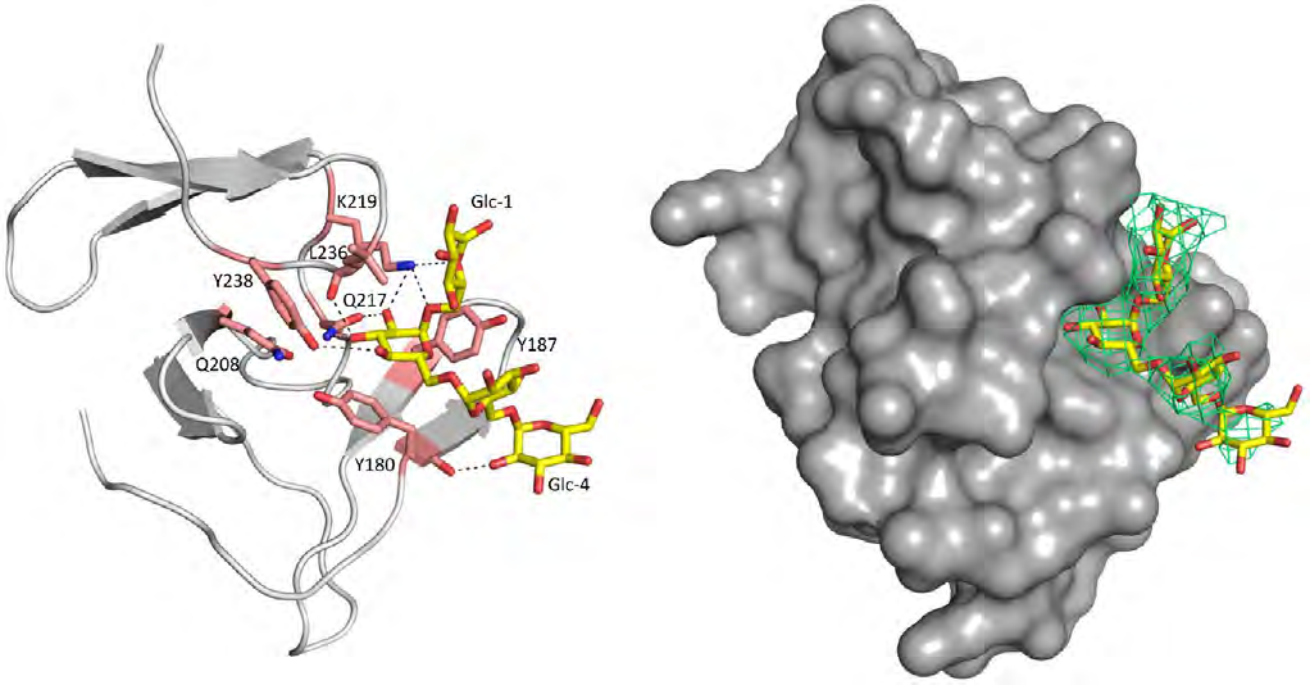

Figure 9. Binding pocket V-A found in the GBD of DSR-MΔ2. An isomaltotetraosyl residue is shown as yellow sticks. The network of hydrogen bonding is shown on the left panel, whereas the electron density map around carbohydrates is displayed on the right panel. The residues involved in binding are represented as pale red sticks (left panel). The difference electron density map ($F_o - F_c$) around carbohydrates was contoured at 3σ (in green).

long loop emerging from the C-term part of domain B from 2731 to 2796 (Figure 6).

Domain IV of DSR-MΔ2 superimposes well with the corresponding domain of GTF180-ΔN (rmsd 1.2 Å on Cα), and secondary structure elements are well conserved except for a β-hairpin (residues 547−560) at the N-terminal border between domains IV and B, unique to DSR-MΔ2.

Domain V of DSR-MΔ2 (5LFC), comprising the first 249 and the last 117 residues located respectively at the N- and C-term ends of the protein, adopts the same orientation as in ΔN123-GBD-CD2 and in the orthorhombic apo form of GTF180-ΔN (PDB entry: 4AYG[50]), with its extremities pointing to the catalytic $(\beta/\alpha)_8$ barrel. Our structure of the DSR-MΔ2 E715Q:I4 complex, including residues 171−1435 and hence the largest domain V solved so far, shows a similar

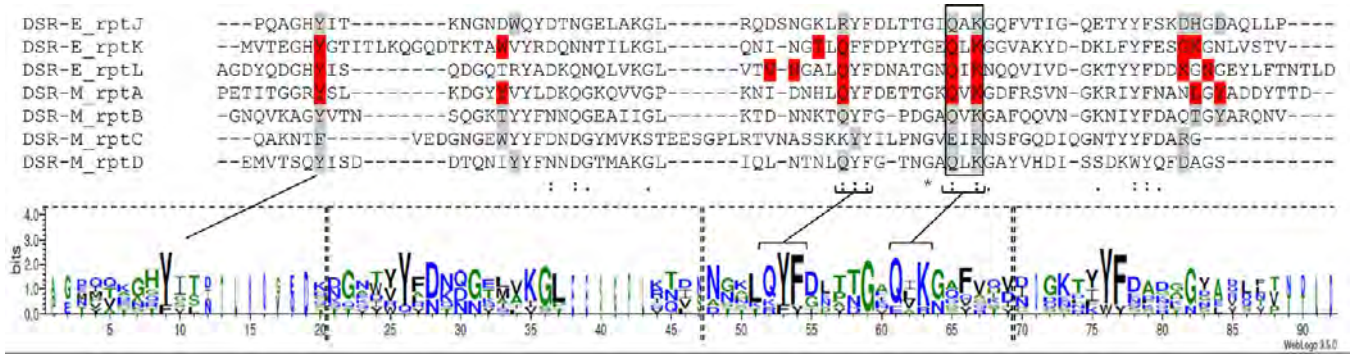

Figure 10. Sequence alignment of the three repeats identified in the GBD of ΔN123-GBD-CD2 (from DSR-E) with those identified in DSR-MΔ2 representing putative glucan binding pockets. Red highlighted residues are involved in sugar binding in repeats K and L of ΔN123-GBD-CD2 (DSR-E) and A of DSR-M, whereas gray highlighted residues are proposed to play the same role in other repeats. The "QxK" motif is framed. A LOGO sequence based on this alignment is shown. The YG repeats are framed in dashed lines on the LOGO sequence.

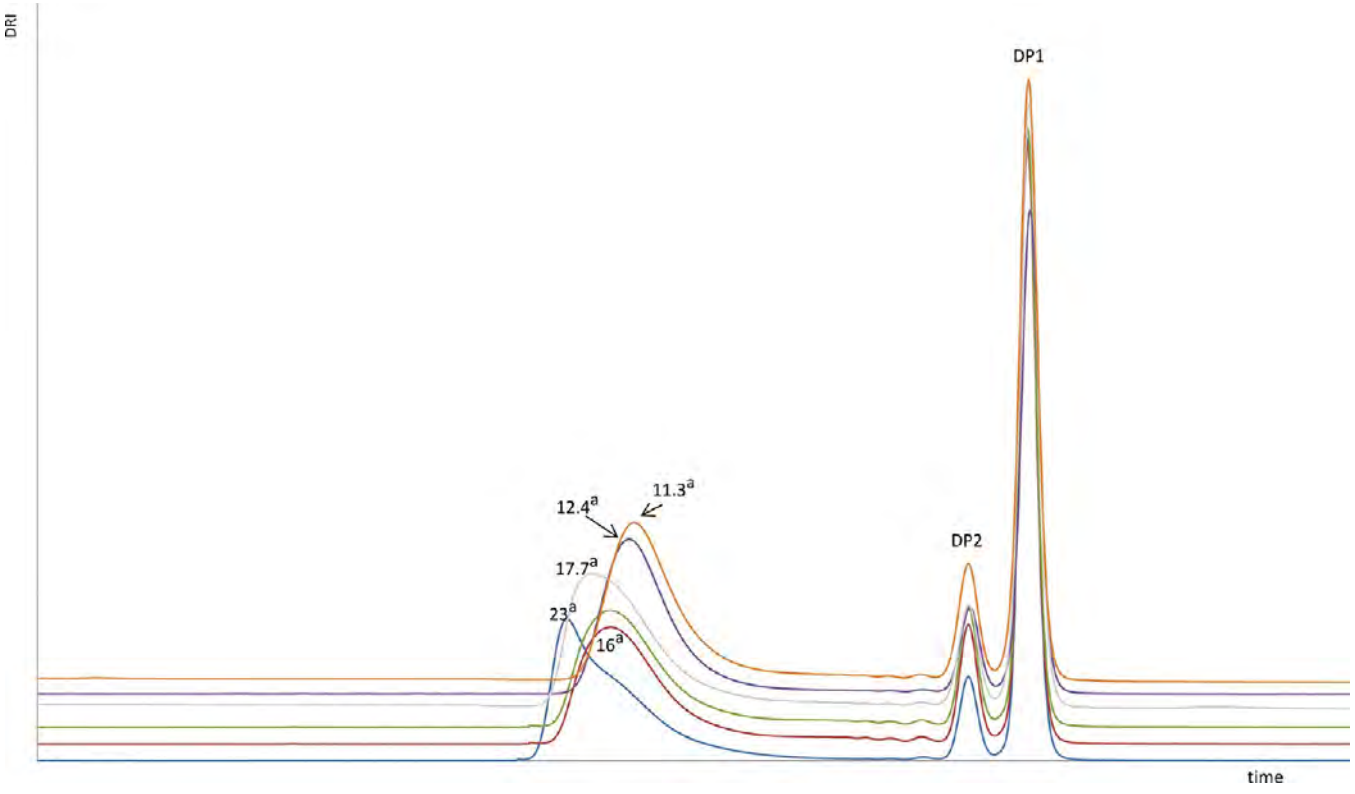

Figure 11. HPSEC analysis of the products synthesized by DSR-M domain V variants from 292 mM sucrose: blue, DSR-MΔ2; red, DSR-MΔV; green, DSR-MΔV-Nter; gray, DSR-MΔ2-Y264A; purple, DSR-MΔ2-Y180A; orange, DSR-MΔ2-YY180−264AA. Legend: (a) determined molar mass at peak apex in kg mol^{-1}.

orientation for domain V. Residues 178−179 and 194−195 at its tip are located at a short distance of 5 Å to helix α6 and α7 of the central $(\beta/\alpha)_8$ barrel that harbors the catalytic site. Several praseodymium ions that intercalate in the crystal packing potentially help to stabilize this domain V. The observation that the GBD is well structured in the E715Q:I4 complex crystal structure, but not in the two other structures presented, prompted us to investigate the solution structure of DSR-M by small-angle X-ray scattering (SAXS). SAXS curves qualify DSR-MΔ2 as a monomeric protein with a radius of gyration (R_g) of 40 Å and a maximum interparticle distance (D_{max}) of ∼125 Å, closely matching the theoretical values calculated from the crystal structure of the I4 complex (39.5 and 117 Å, respectively) (Figure 8). Indeed, rigid-body fitting of the crystal structure, with modeling of flexible N- and C-termini, resulted in a good fit to the experimental data (X = 1.8), suggesting that the observed crystal conformation is highly probable in solution. On the other hand, on observation of the ab initio SAXS envelope, it seems that the protein in solution adopts a "horseshoe" shape with the bend point located between domains IV and V. Although we could imagine a certain flexibility of the domain V, the Kratky analysis suggests that the particle is globally quite compact.

Functional Implications of Domain V. We observed a large part of domain V in the structure of the DSR-MΔ2 E715Q:I4 complex, and we could attribute residual electron density to an isomaltotetraosyl residue (Figure 9) in a pocket named pocket V-A comprising residues 172−245 of domain V.

This pocket adopts a topology similar to that of the sugar binding pockets recently characterized[35] in the branching enzyme ΔN123-GBD-CD2. With all the precautions that should be taken considering the low resolution of our structure, our data enabled the identification of an aromatic residue (Tyr180) in a stacking interaction with the second glucosyl unit of the oligosaccharide (Glc-2, numbering starting from the reducing end). In addition, the O2 atom of Glc-2 also interacts with Gln217 and Lys219, its O3 atom with Gln208, Gln217, and Leu236 (via the oxygen atom of its main chain carbonyl group), and its O4 atom with Tyr238. The side chain of Lys219 also interacts with the oxygen atom of the osidic bond between Glc-1 and Glc-2 and with the O5 of Glc-1. Glc-3 seems to be weakly stabilized by van der Waals interactions with Tyr180 and Tyr187. Finally, the O2 atom of Glc-4 interacts with Tyr180 (via the oxygen atom of its main chain carbonyl group). Sequence alignments of DSR-M domain V with the repeats corresponding to the binding pockets of DSR-MΔ2 and ΔN123-GBD-CD2 (Figure 10) allowed the identification of three other repeats that we designate as repeats V-B, -C, and -D (Figures 1 and 10). Despite the low resolution, our data indicate that pocket V-A and putative pockets V-B and V-C share a similar topology (Figure S6 in the Supporting Information). However, in putative pocket V-C, the residues equivalent to the conserved Tyr180, Gln217, and Lys219 of pocket V-A are replaced by Phe1342, Glu1387, and Arg1389. The dextran binding ability was further investigated by affinity gel electrophoresis in the presence of 68.4 kg mol^{-1} dextran (Figure S7 in the Supporting Information). Similar to the case for ΔN123-GBD-CD2, a clear delay of migration was visualized for DSR-MΔ2, while no significant delay was observed for a construct devoid of the repeats (DSR-MΔV, see below). Finally, DSR-MΔ2 affinity for I6 (used in crystallization assays) was corroborated by ITC analysis, which gave an approximate K_{dI6} value of 10 mM (Figure S7).

To assess the contribution of domain V to the polymerization process, we further truncated DSR-MΔ2 and deleted the putative sugar binding pockets V-A and V-B located at the N-terminal part of domain V (DSR-MΔV-Nter, residues 421−1433, Figure 1). With specific activity (70 U mg^{-1} of protein) comparable to that of DSR-MΔ2, the molar mass of the dextran polymers produced by DSR-MΔV-Nter from 292 mM sucrose (16 kg mol^{-1}) was significantly lower than that of DSR-MΔ2 dextran (23 kg mol^{-1}) (Figure 11 and Table S3 in the Supporting Information) without affecting the protein polymer synthesis ability (still 85% of glucosyl units transferred into dextran). In a second construct, domain V including the putative sugar binding pocket V-C was removed (DSR-MΔV, positions from 421 to 1315, Figure 1). Again, DSR-MΔV retained a specific activity of 70 U mg^{-1} of protein, and 85% of the glucosyl residues from sucrose were incorporated into dextran polymers of 16 kg mol^{-1} (Figure 11 and Table S3). The additional removal of the putative C-terminal pocket V-C hence did not affect the size of the dextran produced. Finally, HPSEC analysis of the acceptor reaction products obtained from 39 kg mol^{-1} commercial dextran and 292 mM sucrose shows that both DSR-MΔ2 and DSR-MΔV enzymes, in addition to the ab initio synthesis produced directly from sucrose, are able to further glucosylate exogenous dextran molecules to a high polymerization degree that is slightly lower for DSR-MΔV than for DSR-MΔ2 (Figure S8 in the Supporting Information).

Because truncation of the putative binding repeats might have a long-range effect by destabilizing the horseshoe structure, we mutated individual amino acids implicated directly in the sugar binding. Tyr180 and Tyr264 of pocket V-A and pocket V-B were obvious candidates for mutation, and we constructed two single mutants (DSR-MΔ2-Y180A, DSR-MΔ2-Y264A) and one double mutant (DSR-MΔ2-YY180-264AA). The single mutation in the pocket V-A (DSR-MΔ2-Y180A) had a pronounced effect on the final dextran size, even more important than the deletion of the whole domain V, with dextrans of only 12 kg mol^{-1} versus 16 kg mol^{-1} for DSR-MΔV (Figure 11 and Table S3 in the Supporting Information). The single mutant DSR-MΔ2-Y264A (mutation in pocket V-B) produced dextrans of 18 kg mol^{-1} molar mass, also contrasting with the 23 kg mol^{-1} of DSR-MΔ2 dextran. The double mutant (DSR-MΔ2-YY180-264AA) produced dextran chains comparable to those of the DSR-MΔ2-Y180A single mutant, with only a marginal additional decrease for the mean molar mass of the resulting dextrans.

DISCUSSION

In comparison with the other characterized glucansucrases from the GH70 family, DSR-M from *L. citreum* NRRL B-1299 is presently the sole enzyme able to produce, from sucrose, only short dextrans of low molar mass. It furthermore presents an excellent efficiency, with 85% of the transferred glucosyl units being incorporated into polysaccharides. DSR-M hence appears as a good enzyme for the production of LMM dextrans directly from sucrose in a single-step, eco-friendly process. Why DSR-M limits the polymerization process to the synthesis of dextran chains of around 30 kg mol^{-1} molar mass whereas other dextransucrases such as DSR-S vardel Δ4N or GTF-180ΔN produce polymer chains of more than several millions of g mol^{-1} was the central question addressed in this study.

For semiprocessive enzymes such as DSR-S vardel Δ4N,[23] HMM polymers (10^8 g mol^{-1}) can already be observed at the early stage of synthesis. For DSR-MΔ2, the polymer size gradually increases with time, indicating a chain elongation mode typical of distributive enzymes. We further show that, during the first 10 min of the reaction, sucrose serves as a primer and velocity is low and constant. After this initial stage, the sucrose-consumption rate increases 4-fold and remains constant until substrate depletion (Figure 3). This reveals that glucosylation of long-chain acceptors is faster than that of sucrose or glucose and further suggests that enzyme deglucosylation may be more efficient in the presence of acceptors of a superior length. However, above a certain size, the length of the acceptor chain does not further affect the glucosyl transfer velocity, explaining why the sucrose consumption remains constant and reflecting the extreme efficiency of DSR-MΔ2 to elongate oligodextrans. Overall, from this biochemical analysis, the ability of DSR-M to produce exclusively LMM dextran could be attributed to (i) a high propensity to use sucrose as both donor and acceptor at the early stage of the reaction, thereby generating a high number of growing dextran chains, and (ii) an equivalent ability to elongate oligodextrans irrespective of their size. The X-ray structures of the enzyme and the inactive mutant DSR-MΔ2 E715Q were solved. Globally, DSR-MΔ2 is structurally organized in five domains, as is the case for the other GH-70 enzyme structures solved so far. However, in domain A, several loops surrounding the catalytic cleft are different from those exhibited by the other GH70 enzymes. Inserted between the

two helices of the H1−H2 subdomain, loop A1 of DSR-MΔ2 is atypical (Figures 6 and 7). Interestingly, sucrose accommodation in the active site induces a reorientation of the Gln794 side chain and leads to a motion of the complete H1−H2 subdomain. Such a motion was already observed for ΔN123-GBD-CD2 in complex with isomaltosyl residues (4TTU)[35] and the equivalent glutamine in GTF-180ΔN (Gln1140) was shown to be implicated in linkage specificity, molar mass, and branching of the produced polymer.[51] In DSR-MΔ2, it could assist sucrose accommodation, fructose release, and acceptor positioning and reflects the functional importance of loop dynamics during catalysis. Loop B1 is another important loop, located at the upper part of the catalytic cleft and near the acceptor subsite +1. In GTF180-ΔN, loop B1 residues Leu938 and Leu940 were shown to influence the linkage specificity, hydrolysis activity, and polymer size.[49] The mutation of Leu575 in DSR-MΔ2 (equivalent to Leu940 of GTF-180ΔN) reduced by 50% the polymer size, indicating a possible role of this residue and by extension of loop B1 in dextran acceptor accommodation. Finally, loop B2 contributes to the width of the binding cleft: either open, as in GTF180-ΔN and GTFA-ΔN, or more compact, as in GTF-SI and DSR-MΔ2. In DSR-MΔ2, it is exceptionally long, potentially contributing to the protection of the glucosyl-enzyme intermediate from water attack and thereby favoring transglucosylation. Indeed, sucrose hydrolysis by DSR-MΔ2 is really minor (3%) in comparison to 24% and 10% for the reactions catalyzed by GTF180-ΔN and GTFA-ΔN, respectively.[49,52] Clearly, the loops shaping the catalytic cavity are determinant for the efficacy and specificity of DSR-MΔ2 and could represent interesting targets for further enzyme engineering.

The X-ray-structure of the entire domain V of DSR-MΔ2 inactive mutant was determined, in complex with I4 (Figure 4). In the crystal, the enzyme looks like a horseshoe, and the SAXS data in solution indicate that this is not a crystallization artifact but rather reflects the flexibility of domain V, as previously demonstrated for GTF180-ΔN.[50] The proximity of domain V to the active site indicates a possible interplay of these two domains, which is further supported by the identification of an IMOS binding pocket at the N-term of DSR-MΔ2. This is the first structural evidence of carbohydrate−protein interactions in domain V of a polymerase, and the binding pocket resembles that recently identified in the branching sucrase ΔN123-GBD-CD2 in complex with isomaltosyl residues. Residues Tyr180, Gln208, and Lys219 of this V-A pocket interact with different atoms of the oligosaccharide (Figure 9) and play the same role as Tyr1834, Gln1879, and Lys1881 in the pocket V-K of the branching sucrase ΔN123-GBD-CD2.[35] Further sequence and structure analysis of DSR-M domain V enabled the identification of three supplemental candidates as sugar binding pockets (Figure 10). Isothermal titration calorimetry, as well as affinity gel electrophoreses, confirmed that DSR-MΔ2 affinity for dextran chains is mainly mediated by domain V, as no binding to dextran could be detected for DSR-MΔV (Figure S7 in the Supporting Information). However, in comparison to the nanomolar affinity estimated for dextran binding of GTF-I and DSR-S domain V fragments,[30,33] DSR-MΔ2 K_d values were estimated at 10 mM for I6 and 300 μM for 68.4 kg mol^{-1} dextran, respectively, which are extremely high but are in agreement with the nonprocessive character of the enzyme.

Finally, to assess the functional role of this domain V, we compared the enzymatic activity of various truncated or point mutants with that of DSR-MΔ2. Deletion of one or more of the pockets does not affect enzyme specific activity or its polymer synthesis ability. These results contrast with those reported[23,27] for polymerases synthesizing HMM polymers such as DSR-S vardel Δ4N and GTF180-ΔN, for which the deletion of the entire domain V resulted in a quasi-total or 25% loss of activity, respectively. However, elimination of the entire domain V of DSRM-Δ2 causes a reduction of the LMM dextran size distribution from 23 kg mol^{-1} (DSR-MΔ2) to 16 kg mol^{-1} (DSR-MΔV). Binding to domain V thus enhances the ability of the enzyme to synthesize longer chains and suggests that the proximity of domain V to the active site allows a possible interplay of these two domains in enzyme catalysis. As elimination of pockets V-A and V-B in DSR-MΔV-Nter or pockets V-A, V-B, and V-C in variant DSR-MΔV has the same effect on the size of the produced dextrans, pocket V-C at the C-terminal extremity of domain V may not be functional. Closer inspection of its structure and sequence revealed that the QxK motif is replaced by the EIR sequence in this putative pocket. Then, the presence of this motif (QxK) together with the spatial proximity of a Tyr might be a defining signature for a functional binding pocket. The single mutations Y180A of pocket V-A and Y264A of pocket V-B result in mutants producing dextrans of molar mass lower than that of DSR-MΔ2, highlighting the crucial role of the tyrosine in oligosaccharide binding and elongation.

CONCLUSION

Overall, our extensive biochemical and structural analyses reveal that DSR-MΔ2 adopts a clear nonprocessive mechanism—with a preference for sucrose as initial acceptor of D-glucosyl units and then an ability to elongate dextran growing chains irrespective of their size—that could be due to singularities in the loops delineating the catalytic cleft. We also report here the most complete 3D structure of a GH70 family member, with a large part of its domain V solved in complex with an isomaltotetraose molecule. The original horseshoe shape of the global structure reveals a high flexibility of domain V and the identification of several sugar binding pockets proposed to locally increase dextran concentration around the active site for chain elongation. However, their weak binding affinity and low number suggest that anchoring of the nascent dextran chains to DSR-MΔ2 domain V is less important than in HMM dextran synthesizing enzymes such as DSR-S vardel Δ4N, explaining why DSR-MΔ2 is distributive and incapable of producing HMM dextran. Altogether, these findings provide new mutation targets for GH70 enzyme engineering aiming at developing new sustainable processes for tailor-made dextran production.

ASSOCIATED CONTENT

Primers used in the study, X-ray collection data statistics, overview of DSR-M constructions, invertase and dextranase digestions, leucrose and fructose acceptor reactions, HPSEC profiles of DSR-M variant products, structural superposition of putative binding pockets, and affinity assays (PDF)

AUTHOR INFORMATION

Corresponding Authors

*E-mail for M.R.-S.: remaud@insa-toulouse.fr.

*E-mail for C.M.: moulis@insa-toulouse.fr.

ORCID

Magali Remaud-Simeon: 0000-0002-2658-672X

Notes

The authors declare no competing financial interest.

ACKNOWLEDGMENTS

This work was supported in part by the French Ministry of Higher Education and Research and the Agence Nationale de la Recherche (ANR). We gratefully thank Pauline Bondy for enzyme construction and recombinant expression help, Florent Grimaud and Etienne Severac for technical support, and Thibault Craviari for crystallization trial assistance. We are also very grateful for ITC analyses realized by Annabelle Varrot and Emilie Gillon from the structural and molecular glycobiology group, CERMAV-CNRS (Grenoble, France). We greatly acknowledge staff from the European Synchrotron Radiation Facility (ESRF, Grenoble, France), as well as the SWING team of synchrotron Soleil (Gif-Sur-Yvette, France) for SAXS acquisition. We thank the ICEO facility (PICT, Toulouse, France) for providing access to HPLC equipment and protein purification systems. Samuel Tranier and the structural biophysics group of the Integrated Screening Platform of Toulouse (PICT, Toulouse, France) are greatly acknowledged for access to the crystallization facility and for their help in synchrotron data collection.

ABBREVIATIONS

GS, glucansucrase; GH, glycoside-hydolase; DP, degree of polymerization; IMOS, isomaltooligosaccharides (I*x*, isomaltooligosaccharide of DP*x*)

REFERENCES

(1) Cantarel, B. L.; Coutinho, P. M.; Rancurel, C.; Bernard, T.; Lombard, V.; Henrissat, B. *Nucleic Acids Res.* **2009**, *37*, D233−D238.

(2) André, I.; Potocki-Véronèse, G.; Morel, S.; Monsan, P.; Remaud-Siméon, M. *Top. Curr. Chem.* **2010**, *294*, 25−48.

(3) Meng, X.; Gangoiti, J.; Bai, Y.; Pijning, T.; Van Leeuwen, S. S.; Dijkhuizen, L. *Cell. Mol. Life Sci.* **2016**, *73* (14), 2681−2706.

(4) Naessens, M.; Cerdobbel, A.; Soetaert, W.; Vandamme, E. J. *J. Chem. Technol. Biotechnol.* **2005**, *80* (8), 845−860.

(5) Vettori, M. H. P. B.; Blanco, K. C.; Cortezi, M.; Lima, C. J. B.; Contiero, J. *Diálogos Ciênc.* **2012**, *2012* (31), 171−186.

(6) Basedow, A. M.; Ebert, K. H. In *Physical Chemistry*; Springer Berlin Heidelberg: Berlin, Heidelberg, 1977; pp 83−148.

(7) Wolff, I. A.; Mellies, R. L.; Lohmar, R. L.; Hellman, N. N.; Rogovin, S. P.; Watson, P. R.; Sloan, J. W.; Hofreiter, B. T.; Fisher, B. E.; Rist, C. R. *Ind. Eng. Chem.* **1954**, *46* (12), 2605−2610.

(8) Gan, W.; Zhang, H.; Zhang, Y.; Hu, X. *Carbohydr. Polym.* **2014**, *112*, 387−395.

(9) Goulas, A. K.; Cooper, J. M.; Grandison, A. S.; Rastall, R. A. *Biotechnol. Bioeng.* **2004**, *88* (6), 778−787.

(10) Khalikova, E.; Susi, P.; Korpela, T. *Microbiol. Mol. Biol. Rev. MMBR* **2005**, *69* (2), 306−325.

(11) Ölçer, Z.; Tanriseven, A. *Process Biochem.* **2010**, *45* (10), 1645−1651.

(12) Zhang, H.-B.; Gan, W.-W.; Zhang, Y.-Q.; Hu, X.-Q. Synthesis of isomalto-oligosaccharides by using recombinant dextransucrase and Hypocrea lixii dextranase. *J. Chem. Pharm. Res.* **2013**, *5* (11), 49−57.

(13) Dols, M.; Remaud Simeon, M.; Willemot, R.-M.; Vignon, M. R.; Monsan, P. F. *Carbohydr. Res.* **1997**, *305* (3−4), 549−559.

(14) Kothari, D.; Baruah, R.; Goyal, A. *Biotechnol. Lett.* **2012**, *34* (11), 2101−2106.

(15) Paul, F.; Oriol, E.; Auriol, D.; Monsan, P. *Carbohydr. Res.* **1986**, *149* (2), 433−441.

(16) Vujicic-Zagar, A.; Pijning, T.; Kralj, S.; Lopez, C. A.; Eeuwema, W.; Dijkhuizen, L.; Dijkstra, B. W. *Proc. Natl. Acad. Sci. U. S. A.* **2010**, *107* (50), 21406−21411.

(17) Pijning, T.; Vujičić-Žagar, A.; Kralj, S.; Dijkhuizen, L.; Dijkstra, B. W. *Acta Crystallogr., Sect. F: Struct. Biol. Cryst. Commun.* **2012**, *68* (12), 1448−1454.

(18) Ito, K.; Ito, S.; Shimamura, T.; Weyand, S.; Kawarasaki, Y.; Misaka, T.; Abe, K.; Kobayashi, T.; Cameron, A. D.; Iwata, S. *J. Mol. Biol.* **2011**, *408* (2), 177−186.

(19) Brison, Y.; Pijning, T.; Malbert, Y.; Fabre, E.; Mourey, L.; Morel, S.; Potocki-Veronese, G.; Monsan, P.; Tranier, S.; Remaud-Simeon, M.; Dijkstra, B. W. *J. Biol. Chem.* **2012**, *287* (11), 7915−7924.

(20) Moulis, C.; André, I.; Remaud-Simeon, M. *Cell. Mol. Life Sci.* **2016**, *73* (14), 2661−2679.

(21) Bai, Y.; Gangoiti, J.; Dijkstra, B. W.; Dijkhuizen, L.; Pijning, T. *Structure* **2017**, *25*, 231.

(22) Leemhuis, H.; Pijning, T.; Dobruchowska, J. M.; van Leeuwen, S. S.; Kralj, S.; Dijkstra, B. W.; Dijkhuizen, L. *J. Biotechnol.* **2013**, *163* (2), 250−272.

(23) Moulis, C.; Joucla, G.; Harrison, D.; Fabre, E.; Potocki-Veronese, G.; Monsan, P.; Remaud-Simeon, M. *J. Biol. Chem.* **2006**, *281* (42), 31254−31267.

(24) Irague, R.; Rolland-Sabaté, A.; Tarquis, L.; Doublier, J. L.; Moulis, C.; Monsan, P.; Remaud-Siméon, M.; Potocki-Véronèse, G.; Buléon, A. *Biomacromolecules* **2012**, *13* (1), 187−195.

(25) Côté, G. L.; Robyt, J. F. *Carbohydr. Res.* **1982**, *101* (1), 57−74.

(26) Joucla, G.; Pizzut, S.; Monsan, P.; Remaud-Simeon, M. *FEBS Lett.* **2006**, *580* (3), 763−768.

(27) Meng, X.; Dobruchowska, J. M.; Pijning, T.; Gerwig, G. J.; Kamerling, J. P.; Dijkhuizen, L. *Appl. Microbiol. Biotechnol.* **2015**, *99* (14), 5885−5894.

(28) Kingston, K. B.; Allen, D. M.; Jacques, N. A. *Microbiology* **2002**, *148* (2), 549−558.

(29) Monchois, V.; Reverte, A.; Remaud-Simeon, M.; Monsan, P.; Willemot, R. M. *Appl. Environ. Microbiol.* **1998**, *64* (5), 1644−1649.

(30) Komatsu, H.; Katayama, M.; Sawada, M.; Hirata, Y.; Mori, M.; Inoue, T.; Fukui, K.; Fukada, H.; Kodama, T. *Biochemistry* **2007**, *46* (28), 8436−8444.

(31) Lis, M.; Shiroza, T.; Kuramitsu, H. K. *Appl. Environ. Microbiol.* **1995**, *61* (5), 2040−2042.

(32) Mori, T.; Asakura, M.; Okahata, Y. *J. Am. Chem. Soc.* **2011**, *133* (15), 5701−5703.

(33) Suwannarangsee, S.; Moulis, C.; Potocki-Veronese, G.; Monsan, P.; Remaud-Simeon, M.; Chulalaksananukul, W. *FEBS Lett.* **2007**, *581* (24), 4675−4680.

(34) Giffard, P. M.; Jacques, N. A. *J. Dent. Res.* **1994**, *73* (6), 1133−1141.

(35) Brison, Y.; Malbert, Y.; Czaplicki, G.; Mourey, L.; Remaud-Simeon, M.; Tranier, S. *J. Biol. Chem.* **2016**, *291* (14), 7527−7540.

(36) Passerini, D.; Vuillemin, M.; Ufarté, L.; Morel, S.; Loux, V.; Fontagné-Faucher, C.; Monsan, P.; Remaud-Siméon, M.; Moulis, C. *FEBS J.* **2015**, *282* (11), 2115−2130.

(37) Wang, W.; Malcolm, B. A. *Biotechniques* **1999**, *26* (4), 680−682.

(38) Studier, F. W. *Protein Expression Purif.* **2005**, *41* (1), 207−234.

(39) Vuillemin, M.; Claverie, M.; Brison, Y.; Séverac, E.; Bondy, P.; Morel, S.; Monsan, P.; Moulis, C.; Remaud-Siméon, M. *J. Biol. Chem.* **2016**, *291* (14), 7687−7702.

(40) Miller, G. L. *Anal. Chem.* **1959**, *31* (3), 426−428.

(41) Kabsch, W. *Acta Crystallogr., Sect. D: Biol. Crystallogr.* **2010**, *66* (2), 125−132.

(42) Winn, M. D.; Ballard, C. C.; Cowtan, K. D.; Dodson, E. J.; Emsley, P.; Evans, P. R.; Keegan, R. M.; Krissinel, E. B.; Leslie, A. G. W.; McCoy, A.; McNicholas, S. J.; Murshudov, G. N.; Pannu, N. S.; Potterton, E. A.; Powell, H. R.; Read, R. J.; Vagin, A.; Wilson, K. S. *Acta Crystallogr., Sect. D: Biol. Crystallogr.* **2011**, *67* (4), 235−242.

(43) McCoy, A. J.; Grosse-Kunstleve, R. W.; Adams, P. D.; Winn, M. D.; Storoni, L. C.; Read, R. J. *J. Appl. Crystallogr.* **2007**, *40*, 658−674.
(44) Emsley, P.; Lohkamp, B.; Scott, W. G.; Cowtan, K. *Acta Crystallogr., Sect. D: Biol. Crystallogr.* **2010**, *66*, 486−501.
(45) Murshudov, G. N.; Vagin, A. A.; Dodson, E. J. *Acta Crystallogr., Sect. D: Biol. Crystallogr.* **1997**, *53*, 240−255.
(46) Bizien, T.; Durand, D.; Roblin, P.; Thureau, A.; Vachette, P.; Pérez, J. *Protein Pept. Lett.* **2016**, *23* (3), 217−231.
(47) David, G.; Pérez, J. *J. Appl. Crystallogr.* **2009**, *42* (5), 892−900.
(48) Petoukhov, M. V.; Franke, D.; Shkumatov, A. V.; Tria, G.; Kikhney, A. G.; Gajda, M.; Gorba, C.; Mertens, H. D. T.; Konarev, P. V.; Svergun, D. I. *J. Appl. Crystallogr.* **2012**, *45* (2), 342−350.
(49) Meng, X.; Dobruchowska, J. M.; Pijning, T.; Lopez, C. A.; Kamerling, J. P.; Dijkhuizen, L. *J. Biol. Chem.* **2014**, *289* (47), 32773−32782.
(50) Pijning, T.; Vujičić-Žagar, A.; Kralj, S.; Dijkhuizen, L.; Dijkstra, B. W. *FEBS J.* **2014**, *281* (9), 2159−2171.
(51) Van Leeuwen, S. S.; Kralj, S.; Eeuwema, W.; Gerwig, G. J.; Dijkhuizen, L.; Kamerling, J. P. *Biomacromolecules* **2009**, *10* (3), 580−588.
(52) Meng, X.; Dobruchowska, J. M.; Gerwig, G. J.; Kamerling, J. P.; Dijkhuizen, L. *Carbohydr. Res.* **2015**, *414*, 85−92.